Additive Manufacturing 50 (2022) 102518

Contents lists available at ScienceDirect

Additive Manufacturing

journal homepage: www.elsevier.com/locate/addma

Effect of extrusion and fused filament fabrication processing parameters of recycled poly(ethylene terephthalate) on the crystallinity and mechanical properties

Babs Van de Voorde [a,c,1], Amalia Katalagarianakis [b,c,1], Sofie Huysman [d], Antoniya Toncheva [e], Jean-Marie Raquez [e], Ivica Duretek [f], Clemens Holzer [f], Ludwig Cardon [g], Katrien V. Bernaerts [h], Danny Van Hemelrijck [b], Lincy Pyl [b], Sandra Van Vlierberghe [a,*]

[a] Polymer Chemistry and Biomaterials Group (PBM), Centre of Macromolecular Chemistry (CMaC), Department of Organic and Macromolecular Chemistry, Ghent University, Krijgslaan 281 S4-bis, B-9000 Ghent, Belgium
[b] Department of Mechanics of Materials and Constructions (MeMC), Vrije Universiteit Brussel, Pleinlaan 2, B-1050 Brussels, Belgium
[c] SIM vzw, Technologiepark 935, B-9052 Zwijnaarde, Belgium
[d] Centexbel, Etienne Sabbelaan 49, B-8500 Kortrijk, Belgium
[e] Laboratory of Polymeric and Composite Materials, University of Mons, 23 Place du Parc, B-7000 Mons, Belgium
[f] Chair of Polymer Processing, Montanuniversität Leoben, Otto Glöckel-Strasse 2, 8700 Leoben, Austria
[g] Centre for Polymer and Material Technologies (CPMT), Department of Materials, Textiles and Chemical Engineering, Ghent University, Technologiepark 130, B-9052 Zwijnaarde, Belgium
[h] Aachen-Maastricht Institute for Biobased Materials (AMIBM), Maastricht University, Urmonderbaan 22, 6167RD Geleen, The Netherlands

ARTICLE INFO

Keywords:
Recycled poly(ethylene terephthalate)
Fused filament fabrication
Melt extrusion
Crystallinity degree
Mechanical properties

ABSTRACT

The production of plastic has grown exponentially over the past few decades and with it the amount of plastic waste leaking in the environment, where it fragments into micro- and nanoplastics. This problematic situation stresses the need for increased plastic collection, recycling and reuse rates. Extrusion-based additive manufacturing (AM) and especially fused filament fabrication (FFF) offer an efficient and effective method to reuse and upcycle recycled plastic. This study focuses on poly(ethylene terephthalate) (PET), which has a broad application window and its recycling is therefore environmentally and economically favorable and sustainable. Therefore, this study involves the thermal and mechanical behavior of recycled PET after extrusion and 3D printing. The extrusion parameters are optimized by performing a complete physico-chemical and thermal analysis of the obtained filaments and they were compared with commercial virgin and recycled PET. Moreover, the influence of the applied processing conditions on the degree of crystallinity and mechanical properties is investigated. The filaments are then used for FFF, where various printing parameters are altered to obtain the optimum printing conditions (i.e. printing temperature, the build plate temperature, fan cooling and printing directions). The effect of the degree of crystallinity of semi-crystalline PET is investigated via altered printing parameters, showing superior mechanical properties for an increasing degree of crystallinity. To verify the portability of the obtained optimized print parameters, two different FFF printers are used. The use of recycled PET as feedstock for FFF supports the efforts for improving the sustainability of plastics by valorizing PET waste, and prolonging the lifecycle of PET.

1. Introduction

In modern life, polymers are indispensable because of their broad application potential in the fields of packaging, automotive, building and construction. To meet the demand, the plastic production is rapidly increasing, and reached 350 million tons worldwide and 61.8 million tons in Europe in 2018.[1] The latter has prominent consequences for nature as the plastic waste stream is also increasing, both in landfills and

* Corresponding author.
E-mail address: Sandra.VanVlierberghe@UGent.be (S. Van Vlierberghe).
[1] Both authors contributed equally.

https://doi.org/10.1016/j.addma.2021.102518

Available online 27 November 2021

in the ocean.[2,3] It is expected that the weight of plastic in the ocean will be more than the weight of fish by 2050 if no actions are taken.[2] In order to avoid plastic waste entering the ocean and to achieve a circular economy of plastics, increasing attention is being paid to the collection of plastics and to use them for energy recovery and recycling. In 2018, 29.1 million tons were collected in Europe, of which 42.6 % was used for energy recovery and 32.5 % was recycled, while 24.9 % was disposed into a landfill.[1] The largest end-user market for polymers is packaging, which mainly includes polyethylene (PE), polypropylene (PP) and poly(ethylene terephthalate) (PET). In 2018, 42 % of the collected packaging waste in Europe was recycled, while a higher recycling target of 50 % has been set for 2025.

As PET is used in many applications such as packaging, fibers for clothing, automotive parts and in various biomedical applications, its recycling is environmentally favorable and sustainable.[4–7] In order to fulfil the recycling target of 50 % by 2025, lower grade products are currently made from plastics, including carpets and fiber filling for pillows from PET bottles.[8] PET can be reused after a thorough cleaning step or mechanically recycled into recycled PET (rPET) pellets or even mixed with virgin PET (vPET) to assure a higher quality.[9,10] Furthermore, chemical recycling into monomer units is also one of the many recycling possibilities.[11].

Another way of valorizing plastic waste is to reprocess it to prolong the life-time of the material. Reprocessing PET towards recycled end-products could be performed by various techniques, including compression molding, film extrusion or injection molding.[12,13] Besides the listed processing techniques, PET could also be reprocessed into a filament via melt extrusion, which could thereafter be used as feed for fused filament fabrication (FFF).[14,15] FFF is a versatile technique with many advantages, including manufacturing various parts with high complexity and resolution on-demand within a reduced lead time and at reduced cost compared to compression molding or injection molding. More specifically, FFF is one of the most cost-effective extrusion-based additive manufacturing (AM) processes, which generates parts in a layer-by-layer fashion according to a computer-aided design (CAD). FFF has a selective pool of available filaments, including recycled polymers and is therefore considered to be an efficient fabrication method.[16,17] Recycled polymer filaments are already commercialized by several companies. However, although these companies claim to sell recycled PET filaments, the multitude of these filaments are poly(ethylene terephthalate glycol) (PETG), which is similar in chemical structure to PET, except for part of the ethylene group that is replaced by cyclohexanedimethylene, resulting in a copolymer with a lower crystallization degree. Companies which commercialize filaments that are completely based on recycled plastics are Refil, 3DJake and Tridea, among others. More specifically, Refil produces a 100 % recycled acrylonitrile butadiene styrene (ABS) filament from car dashboards, while 3DJake sells 100 % recycled polylactic acid (PLA) and PETG. Tridea provides recycled PET filaments from PET bottles.

As opposed to subtractive manufacturing, the waste during production is very limited within AM. Besides plastics, also metals, composites and biological materials can be used as feedstock. AM has already found its entry in multiple industries, including automotive, aerospace and in medical applications.[15,18] Although AM has many advantages, one of the disadvantages is the selective pool of available filaments for FFF, especially the limited availability of semi-crystalline polymer filaments.[19–23] The latter show multiple advantages over amorphous polymers including generally higher melting temperatures compared to the amorphous glass transition temperature (T_g), improved chemical resistance and mechanical properties, including tensile modulus, strength, toughness and wear resistance.[24] The fact that semi-crystalline materials are rarely used as feedstock for FFF is due to their crystallinity, resulting in shrinkage and warpage during 3D printing.[24–26] After deposition, the polymer is cooling down due to the large thermal gradient between the heated nozzle and the build plate temperature, which results in a decrease of the free volume when the temperature is still above the glass transition temperature. This will result in thermal contraction or shrinkage and the printed object will detach from the build plate. Shrinkage is mostly occurring for semi-crystalline materials as their volume decreases drastically during crystallization because the formed crystals are denser compared to amorphous materials. In order to minimize shrinkage and warpage, crystallization is therefore avoided during the cooling process in 3D printing, although the formed crystals influence the mechanical properties drastically. Due to the alignment of the ordered crystals and the stronger intermolecular forces, a higher strength and modulus are obtained for the printed parts. Previously, this phenomenon was investigated by Yang *et al.* (2017), who evaluated the influence of the thermal processing conditions on the crystallinity and mechanical properties of 3D printed parts of semi-crystalline poly(ether ether ketone) (PEEK).[20] With an increasing ambient and nozzle temperature, the crystallinity and therefore the tensile modulus and tensile strength increased.

In literature, several semi-crystalline polymers have already been investigated as feedstock for FFF, including PEEK, PP and PET.[19–21,27,28] Although 3D printing with PET has already been described in literature, the focus was mainly on the possibility to recycle the material, while a complete investigation of the crystallinity during extrusion and 3D printing is lacking. Therefore, this study is mainly focused on the thermal behavior of rPET during extrusion and 3D printing. Moreover, the mechanical properties of the extruded filament and printed parts were thoroughly investigated via tensile testing.

As stated earlier, recycling is gaining increasing attention and applications using rPET are endless. Therefore, a commercially available rPET filament from Tridea that was mechanically recycled, was included herein to compare its characteristics with vPET. A complete analysis was performed, including physico-chemical and thermal analysis of the filaments and their mechanical properties were compared. Moreover, rPET pellets were used to investigate the extrusion conditions and the influence of the applied processing parameters on the thermal and mechanical properties of the filaments. Furthermore, the printing conditions of the Ultimaker 3 FFF printer were altered to obtain the optimum processing parameter set, including the printing temperature. As PET is semi-crystalline and prone to shrinkage, the influence of the build plate temperature was investigated and optimized. How crystallinity affected the tensile modulus was assessed via combinations of various printing and build plate temperatures during printing. To examine the interface between the printed tracks and the polymeric diffusion across the interface, the samples were printed in different directions, namely parallel and perpendicular to the load and tested via tensile testing, while void analysis was performed via optical microscopy images of polished sampled. Lastly, two FFF printers were applied and compared, namely Ultimaker 3 and Prusa i3, to investigate whether the direct translation of all optimized printing parameters from one device to another was possible.

2. Materials and methods

2.1. Materials

In this study, a commercial vPET filament (Nexeo 3D, 2.85 mm, $vPET_f$) was evaluated and compared with a commercial rPET filament (Tridea, 1.75 or 2.85 mm, $rPET_f$), which was mechanically recycled. For the investigation of the extrusion capabilities of recycled PET, mechanically recycled PET pellets were applied (Tridea, $rPET_p$). The mechanical recycling of $rPET_f$ and $rPET_p$ was performed by the same company, which keeps the recycling conditions confidential. Moreover, 1,1,1,3,3,3-hexafluoro isopropanol 99.9 % from Evochem and sodium trifluoroacetic acid from Sigma-Aldrich were used for size exclusion chromatography (SEC), while trifluoroacetic acid-d 99.5 % was purchased from Sigma-Aldrich and was applied as solvent for proton nuclear magnetic resonance (^{1}H NMR) spectroscopy.

2.2. Polymer characterization

The chemical structure and purity of the filaments were confirmed with ^{1}H NMR spectroscopy, using a Bruker AVANCE 300 (300 MHz) and a 400 MHz AVANCE II Ultrashield Bruker. All spectra were measured in trifluoroacetic acid-d and were analyzed with ACD/Labs software. The degradation temperature was determined with thermogravimetric analyses (TGA) using a TA Instruments Q50 operating under nitrogen atmosphere. The samples were heated from 35 °C to 750 °C at a rate of 10 °C/min. The thermograms were analyzed using the TA Universal Analysis software from TA Instruments. Modulated differential scanning calorimetry (mDSC) analyses were performed with a TA instrument Q2000 DSC operating under nitrogen atmosphere at a heating rate of 2 °C/min, a cooling rate of 5 °C/min and modulated with an amplitude of ± 0.32 °C with a 60 s period. The glass transition (T_g) and melting temperature (T_m) were determined based on the heat capacity component, i.e. the reversing heat flow of the second heating curve, while the crystallization (T_c) and cold crystallization temperature (T_{cc}) resulted from the kinetic component, i.e. the non-reversing heat flow of respectively the cooling and the first heating curve. Furthermore, the initial degree of crystallinity (X_c) was calculated via

$$X_c(\%) = \frac{\Delta H_f - \Delta H_{cc}}{\Delta H_f^0} * 100\% \quad (1)$$

where ΔH_f is the enthalpy of fusion, ΔH_{cc} the enthalpy of cold crystallization and ΔH_f^0 the heat of fusion of 100 % crystalline PET (140 J/g), all extracted from the first heating run of respectively the reversing and non-reversing heat flow.[29] All required info was determined using the TA Universal Analysis software from TA Instruments. The mDSC measurements were performed in a temperature range between 0 °C and 300 °C. Furthermore, the molar mass and the polymer dispersity were determined with size exclusion chromatography (SEC). To this end, in 1.5 ml 1,1,1,3,3,3-hexafluoro isopropanol containing 0.019 % sodium trifluoroacetate, 5 mg of the PET materials was dissolved and filtered over a 0.2 μm Teflon syringe filter. For the calibration curve, poly(methyl methacrylate) standards with a molar mass ranging from 831 to 1 890 000 g/mol were used. First, a pre-column PFG combination medium with 7 μm particle size (4.6 x 30 mm) was used and thereafter two PFG combination medium microcolumns with 7 μm particle size (4.6 x 25 mm, separation range 100 – 1 000 000 g/mol), in combination with a refractive index detector. The spectra were analyzed with the PSS WinGPC UniChrom software.

2.3. Extrusion of rPET filaments

The recycled PET pellets were dried before extrusion in a vacuum oven at 80 °C. Two setups were used operating at different capacity and extrusion speed, as outlined below:

2.3.1. DSM vertical micro compounder 15 ml HT

Recycled PET pellets were introduced into the twin-screw DSM vertical micro compounder, which has a capacity of 15 ml. The temperature ranged from 270 °C to 275 °C, while the twin screw rotated with a speed of 30 rpm under nitrogen flow. When all the material was added, the speed was increased to 60 rpm and the mixing proceeded during the next 3 or 5 min. Then, a speed of 5 rpm was applied and, depending on the die, filaments with a diameter of 1.75 or 2.85 mm were extruded.

2.3.2. FET Monofilament and tape extrusion line (2.5 – 5 kg/h)

Recycled PET pellets were added to the monofilament extrusion line (Fibre Extrusion Technology Ltd), which has a capacity of 2.5 – 5 kg/h. After an optimization process, a temperature profile of 250–270–280–285 °C for the four zones was selected instead of 220–230–250–250 °C, while the pressure of the extruder was 45 bar. The use of a filter was avoided and a spinneret with one circular hole of 5 mm diameter was used and depending on the required filament diameter of 1.75 or 2.85 mm, the rotation speed during extrusion was respectively 12.3 or 24.3 rpm. A water bath with a temperature of 30 °C was placed at the end of the extruder. The diameter and roundness were monitored with a Sikora Ecocontrol device and depending on the obtained data, the speed and throughput was adapted to obtain the required dimensions.

2.4. Fused filament fabrication with PET

Before and during printing, the filament was kept in a box at a controlled humidity of 20 % and a temperature of 30 °C. As FFF printers, Ultimaker 3 and Prusa i3 MK3S were used and various parameters were evaluated using the Ultimaker 3 as summarized in Table 1, to identify the optimal printing conditions. The nozzle temperature was varied from 240 °C to 275 °C, while the build plate temperature ranged from 40 °C to 100 °C. The sample geometry was based on ASTM standard D3039, except for the overall length of the samples, which was reasonably reduced (see Fig. S1, Supporting information).[30] Therefore, rectangular parts with dimensions 165 x 25 x 2.5 mm^3 were printed. Samples with printing directions parallel to the load [0°] and transverse to the load [90°] were studied. Typically, top and bottom layers with a printing direction of ± 45° and a layer wrapping around the samples are printed by default in a dense pattern for improved surface quality of the part. As these layers would not enable to measure the effect of the printing orientation, they were not included in the CAD design. Moreover, each printer has its own slicer software to convert the STL file into the corresponding G-code. Although the default settings would be identical, the G-codes could vary. Therefore, the G-code was generated with the same slicer, here via the Cura 3.3.1 software.

2.5. Mechanical characterization

2.5.1. Tensile tests on filaments

The tensile tests on single filaments were performed with the Tinius Olsen 5ST. The device was equipped with a 500 N load cell and 7 filament pieces were tested within each series. The filament was placed between two clamps which exerted a pressure of 4 bar to avoid slipping. A preload of 0.1 N was selected, while the preload speed was maintained at 1 mm/min. Hereafter, the crosshead had a displacement speed of 10 mm/min and proceeded until failure of the filament. The strain was calculated using the initial gage length of the filament (30 – 40 mm) and the crosshead displacement. The tensile modulus was calculated for each filament and significant differences ($p < 0.05$) were calculated with one-way ANOVA.

2.5.2. Tensile tests on printed parts

Tensile tests were conducted according to the ASTM D3039 standard. For all series, at least five printed tensile parts were tested using an

Table 1
Summary of the printer settings for both Prusa i3 MK3S and Ultimaker 3, including the parameters which were varied to identify the optimal processing conditions.

Printing parameter	Prusa i3 MK3S	Ultimaker 3
Nozzle temperature	260 °C	240–275 °C
Nozzle diameter	0.4 mm	0.4 mm
Build plate temperature	100 °C	40–100 °C
Initial printing speed	20 mm/s	20 mm/s
Printing speed	40 mm/s	40 mm/s
Fan cooling	100 %	0 – 100 %
Layer height	0.1 mm	0.1 mm
Layer width	0.35 mm	0.35 mm
Infill line pattern	[0 °]	[0 °] – [90 °]
Filament diameter	1.75 mm	2.85 mm

Instron 5885 machine which was operated with mechanical grips and a 10 kN load cell. Each tensile test was performed under displacement control at a crosshead displacement rate of 2 mm/min, until final failure. Thick paper end tabs were used to protect the printed parts from the clamping grips. The cross-sectional area was measured for the determination of the mechanical properties of the printed coupons. The width of the samples was measured by a caliper, while the thickness was measured by a micrometer.

To measure the strain of each printed part, a stereo digital image correlation (DIC) system (VIC-3D by Correlated Solutions with two Stingray Cameras of 5 MP and 23 mm lenses) was used (see Fig. S2, Supporting information). For this purpose, a black speckle pattern on a white background was applied to the surface. Two cameras were then focused on the speckled surface of the printed part, taking images every second throughout the duration of the test. A virtual extensometer was used afterwards to extract the longitudinal strain of the part from these images. The tensile modulus was defined as the average value in the 0.1–0.3 % strain range. Significant differences ($p < 0.05$) were calculated with one-way ANOVA.

2.6. Void content determination

In order to compare the effect of different printing directions on the void content and printing accuracy, the void content of all materials was investigated through optical microscopy. Pieces were cut from the printed vPET and rPET samples, which were subsequently sanded and polished. Images were taken over the total cross-section of the tested sample using a Leica MZ12.5 microscope and the images were analyzed using ImageJ. The cross-sectional area of the voids relative to the polymer was measured for each image, and averaged over the total cross-section of the tested samples. For this purpose, a threshold was chosen for each individual image. All pixels with a grey value above the threshold were considered voids, and all pixels below the threshold were considered polymer matrix.

2.7. Pressure-volume-temperature-measurements (pvT)

To analyze the shrinkage during cooling, a PVT100 (SWO Polymertechnik GmbH, Germany) was used according to ISO 17744 [31], which cooled down from 290 ° C to 40 °C at a constant rate of 0.1 °C/s, while the pressure maintained 200 bar. The relative specific volume with respect to the reference value at 40 °C was plotted as a function of the temperature in the temperature range between 40 °C and 290 °C.

2.8. Scanning electron microscopy

Micrographs of the fractured surface after tensile testing were obtained via scanning electron microscopy (SEM) to inspect the failure modes. The specimens were coated with a thin conductive gold layer by an automatic Sputter Coater K550X to avoid charging. The images were obtained with a Phenom Desktop SEM-Fei using two magnifications of 5 000 and 20 000, applying an acceleration voltage of 5 kV.

3. Results and discussion

3.1. Polymer characterization

Polymer recycling can have an enormous impact on the chain length and entanglements, which will subsequently influence the mechanical and thermal properties. Therefore, the mechanically recycled PET filaments and pellets were analyzed to assess their physico-chemical and thermal properties. Two commercial materials were selected as benchmark, including a commercial virgin PET filament from Nexeo 3D (referred to as $vPET_f$) and a recycled PET filament with a filament diameter of 2.85 mm obtained from Tridea (referred to as $rPET_f$), to compare the chemical characteristics with those of rPET pellets from the same company, here named $rPET_p$. The latter were used thereafter for processing the rPET filaments via melt extrusion on both lab and industrial scale.

3.1.1. Chemical characterization of the commercial PET materials

For the chemical characterization, proton nuclear magnetic resonance (^{1}H NMR) spectroscopy was performed on all materials using trifluoroacetic acid-d as solvent (see Fig. 1). The characteristic signal corresponding to the aromatic ring was found as a multiplet around 8.14 ppm (signal a, m, 4 H), while the peak characteristic for the two identical methylene groups was located as a triplet around 4.82 ppm (signal b, t, 4 H). As the ratio of the integrations of the proton peaks is identical with $vPET_f$, the commercial rPET filament and pellets appear to be constituted of pure PET without any additives which indicates that all materials are comparable with regard to chemical composition.

As molar mass is an important characteristic of polymers, in addition to their thermal and mechanical properties, size exclusion chromatography (SEC) was performed (Table 2). Via SEC, the number average molar mass (M_n) and mass average molar mass (M_w) were determined, in combination with their dispersities ($Đ$). The M_w varied from 18000 up to 21400 g/mol, with $vPET_f$ representing the lowest value, while the recycled materials $rPET_f$ and $rPET_p$ were slightly higher. Furthermore, the dispersity ranged from 2.1 to 2.9, which is a common dispersity range for PET synthesized via a step-growth reaction.[32] Here, the results show that the performed mechanical recycling towards $rPET_f$ and $rPET_p$ does not impact the molar mass, nor its dispersity and that the commercial $rPET_f$ is not inferior compared to $vPET_f$. Although various applications of PET do not require high molar masses (i.e. fibers for clothing and films), the chain length could be increased with solid state polymerization during or after recycling.[33–35] Here, the viscosity of the material increases depending on which temperature and reaction time is used, typically ranging respectively from 200 °C to 240 °C and 5–25 h.[9] Via this way, high molar mass PET could be produced for bottle packaging applications and industrial fibers.

3.1.2. Thermal characterization of the commercial PET materials

An in-depth thermal analysis of the PET materials was performed before extrusion via thermogravimetric analysis (TGA) and modulated differential scanning calorimetry (mDSC). The former was used to determine the degradation temperature at the onset point ($T_{d,\ onset}$) (see Table 3). The thermograms show that the same degradation profile is obtained and includes a single step decomposition due to simultaneous breakage of the ester and aliphatic moieties, while the materials are stable up to 350 °C (see Fig. S3, Supporting information).[36,37] As one step is visible, only one type of polymer is present. After decomposition, carbonized materials remain, which ranged between 10 and 15 wt%.

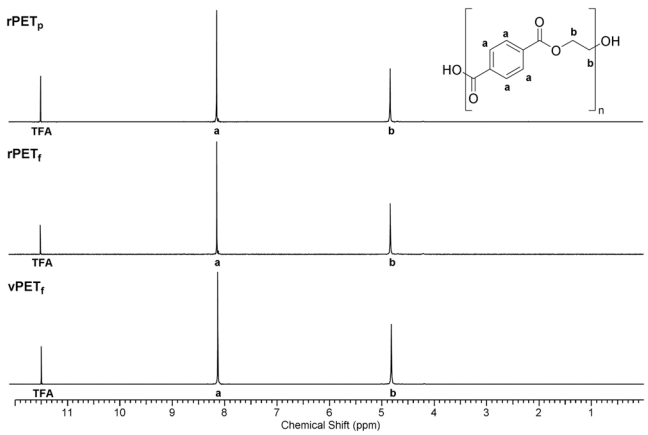

Fig. 1. Overview of ^{1}H NMR spectra of $vPET_f$, $rPET_f$ and $rPET_p$ recorded using trifluoroacetic acid-d as solvent.

Table 2
Molar mass and dispersities were determined with SEC in 1,1,1,3,3,3-hexafluoro isopropanol for the three commercial PET materials.

	M_n [g/mol]	M_w [g/mol]	$Đ$
$vPET_f$	8500	18000	2.1
$rPET_f$	9400	21000	2.2
$rPET_p$	7500	21400	2.9

Table 3
Thermal properties of $vPET_f$, $rPET_f$ and $rPET_p$, including the remaining residue after decomposition with TGA and degree of crystallinity (X_c) measured with mDSC.

	$T_{d,\ onset}$ [°C]	Residue [%]	T_g [°C]	T_{cc} [°C]	$T_{m,1}$ [°C]	$T_{m,2}$ [°C]	T_c [°C]	X_c [%]
$vPET_f$	401	11.5	84	116	249	258	207	22.5
$rPET_f$	400	12.6	80	116	241	250	198	20.4
$rPET_p$	402	14.8	83	/	242	250	201	36.3

The results are in agreement with previous reports in literature.[36,38].

Via mDSC, the glass transition (T_g), the cold crystallization (T_{cc}), the first and second melting ($T_{m,1}$ and $T_{m,2}$) and the crystallization temperature (T_c) were determined (see Table 3). The T_g and T_m were determined based on the heat capacity component, the reversing heat flow, while the T_{cc} and T_c resulted from the kinetic component, the non-reversing heat flow. The results showed that the materials are semi-crystalline and the T_g for all materials is around 80 °C, which is in agreement with literature (see Fig. S4 for $vPET_f$ and $rPET_f$, Supporting information).[33,39] Furthermore, two endotherms were present in the non-reversing heat flow at higher temperatures which is attributed to two different lamella thicknesses produced during crystallization and re-crystallization during melting.[40] In addition, the initial degree of crystallinity (X_c) was measured and varied depending on the processing conditions. As $rPET_p$ requires further processing towards filaments or films, the used extrusion conditions provided pellets with a higher degree of crystallinity compared to the filaments to avoid moisture in the pellets to the greatest extent possible since crystals are considered impermeable to moisture.[41,42] The latter is accomplished on purpose by controlling the extrusion cooling because the presence of moisture could potentially result in a reduction in molar mass through H_2O-induced backbone degradation during further processing.[5,43,44] On the other hand, the virgin and recycled PET filaments are processed in such a way that they exhibit less semi-crystalline regions to facilitate the 3D printing process (i.e. with regard to flexibility and flow properties). Moreover, $rPET_p$ was already fully crystallized during processing, which results in the absence of a T_{cc} in the first heating cycle.

3.2. Extrusion of rPET

3.2.1. Identification of optimal extrusion parameters

In order to investigate the optimal extrusion parameters for rPET on lab scale, a vertical mini twin-screw extruder with a capacity of 15 cm^3 was used to process recycled filaments starting from $rPET_p$. As the filaments were to be used as feed for the Ultimaker 3, filaments with a diameter of 2.85 mm were extruded and therefore the corresponding die was used. First, the temperature of the extruder was fixed at 275 °C in all the extruder zones to ensure an appropriate extrusion flow. Furthermore, based on various reports involving the residence time of various materials during twin-screw extrusion, a mixing time of 5 min was selected.[45–47] Due to the impermeability of crystals for water and the higher degree of crystallinity for $rPET_p$, the initial extrusion testing proceeded without extra drying of the pellets.[41,42] After 5 min of mixing, filaments with an uneven diameter ranging from 1.8 to 3.5 mm were obtained, which is the result of the absence of a diameter controller and spooler (i.e. filament was collected manually). In order to evaluate to what extent the extrusion process impacted the molar mass, SEC was performed (see Table 4). The results showed that blending during 5 min at 275 °C induced a reduction of 51 % in M_w going from 21400 down to 10500 g/mol, which will result in inferior mechanical properties (for example a reduced tensile modulus). It is desired to obtain filaments with a high tensile modulus and strength to ensure the mechanical performance of the printed part.[48] The molar mass degradation is the result of both thermal degradation due to the long exposure to high temperatures and hydrolysis of the ester bonds due to presence of moisture. Thermal analysis was performed to determine the influence of the extrusion process on the degree of crystallinity (see Table 4). The results of mDSC showed that a crystallization degree of 37.6 % was obtained, which was an increase of 85 % compared with that of $rPET_f$ (20.4 %). The increased crystallinity will have a major influence on the stiffness of the filament (i.e. brittle behavior), as known from literature (see 3.2.2.).[13,49–51] The increased crystallinity was also visualized by the opaque color of the filament (see Fig. S5a, Supporting information).[24].

The extrusion conditions were modified in an attempt to decrease the molar mass reduction to promote increased chain entanglements, and obtain filaments with a lower degree of crystallinity, which would be more flexible and therefore more easily processable during 3D printing. Besides thermal degradation of PET, the molar mass also decreases via hydrolysis of the ester bonds and therefore even the slightest amount of moisture should be avoided.[9,34,35] For that reason, the $rPET_p$ pellets were dried prior to extrusion, in a vacuum oven at 80 °C for at least 12 h. In an attempt to further reduce the impact on the molar mass, the blending time and temperature were decreased to respectively 3 min and 270 °C. A further decrease of the temperature was not possible as melting of the pellets was not realized in the latter case. Because of the manual collection of the filaments around a Teflon tube, variations in the filament diameter occurred, ranging from 2.5 to 3.2 mm. Exploiting the new extrusion conditions, a decrease in molar mass was still apparent, albeit less pronounced (i.e. 29 % for $rPET_{275\ °C,\ 3'}$ and 28 % for $rPET_{270\ °C,\ 5'}$ instead of 51 % for $rPET_{275\ °C,\ 5'}$). The dispersity of the extruded filaments was around 2. Via mDSC, crystallinity was measured, which ranged from 20.6 for $rPET_{275\ °C,\ 3'}$ to 25.3 % for $rPET_{270\ °C,\ 5'}$. As both reduction in blending time and temperature were successful, both were combined to obtain the optimal extrusion conditions. In the case of PET, the crystallization degree largely depends on the cooling rate applied. As no cooling was initially applied, a highly crystalline and more brittle filament was obtained. To obtain a more flexible filament, a cooling bath was used subsequently, exploiting ice as cooling medium (5 °C). The mDSC measurements revealed that a lower degree of crystallinity of 17.8 % was obtained and therefore, a more ductile and transparent filament.

The results showed that the lowest possible extrusion temperature should ideally be used, in combination with a short residence time. More importantly, pellets need to be dried prior to extrusion and a water bath of 5 °C should be used to ensure fast cooling after extrusion. With this knowledge, the extrusion of $rPET_p$ was realized on an industrial-scale extruder with four heating zones, which had a higher capacity of 2.5 – 5 kg/h. Various temperature profiles were investigated for the various zones. When the temperature profile was 220–230–250–250 °C with

Table 4
Overview of the SEC results of $rPET_p$ and the extruded rPET filaments on the lab-scale extruder and the degree of crystallinity (X_c) obtained via mDSC.

	M_n [g/mol]	M_w [g/mol]	$Đ$	X_c [%]
$rPET_p$	7500	21400	2.9	36.3
$rPET_{275\ °C,\ 5'}$	5800	10500	1.8	37.6
$rPET_{275\ °C,\ 3'}$	7600	15100	2.0	20.6
$rPET_{270\ °C,\ 5'}$	8200	15400	1.9	25.3
$rPET_{270\ °C,\ 3',\ ice}$	8100	15800	1.9	17.8

220 °C corresponding with the first zone, the pressure was too high, which resulted in a malfunctioning device, while if 250–270–280–285 °C was selected, extrusion was successful. The temperature of the first zone was 250 °C, which was kept low as in this case the pellets did not completely melt, thereby providing enough pressure for the subsequent zones to enable a successful large scale extrusion process. As two FFF printers were used, both filament diameters were extruded, namely 1.75 and 2.85 mm. A diameter controller was placed after the cooling bath, which automatically adjusted the extrusion speed when deviations in diameter occurred. This resulted in smooth and transparent filaments with minor variations in the filament diameter (± 0.1 mm) (see Fig. S5e and f, Supporting information). Via SEC, a M_w of 14 300 and 16600 g/mol for the 1.75 and 2.85 mm diameter filaments, respectively, were obtained, which implies a molar mass degradation equally to the filaments extruded on the lab-scale extruder (see Table 5). The latter was anticipated based on the same residence time of the pellets in the extruder, roughly 3 min. The dispersity in both cases was again ± 2. With mDSC, the crystallinity was assessed and the results showed more amorphous filaments with a crystallinity of respectively 11.8 % and 15.8 % (see Fig. S6 for $rPET_{2.85\ mm}$, Supporting information). Furthermore, Fig. S6 shows that $rPET_{2.85\ mm}$ exhibits the same thermal characteristics when compared to $vPET_f$ and $rPET_f$ represented in Fig. S4 (i.e. glass transition around 80 °C, cold crystallization in the first heating cycle and a double melting peak in the second heating cycle).

3.2.2. Mechanical characterization of the extruded filaments

To obtain the mechanical properties of the extruded filaments, tensile testing on a single filament was performed and $vPET_f$ and $rPET_f$ were selected as benchmark materials. The filaments were elongated until failure and the tensile modulus, ultimate tensile strength and strain are shown in Table 6. In case of the filament processed at 275 °C/5' with a high crystallinity degree of 37.6 %, a brittle fracture was observed as shown by the low ultimate tensile strain of 5.63 ± 3.65 %, while in all other cases, corresponding with lower crystallinity degrees (11.8 – 25.3 %), a ductile fracture was noticed. The average tensile moduli are shown in Fig. 2. For $rPET_{275\ °C,\ 5'}$, a tensile modulus of 1.05 ± 0.16 GPa was obtained, which was not significantly different from the tensile moduli of $rPET_{275\ °C,\ 3'}$ and $rPET_{270\ °C,\ 5'}$, respectively 0.94 ± 0.07 GPa and 0.98 ± 0.15 GPa. It is known from literature that crystallinity has a major influence on the stiffness.[13,49–51] In case of the brittle $rPET_{275\ °C,\ 5'}$, a higher tensile modulus was expected compared to the other filaments due to its higher crystallinity degree. However, no significant difference was noticed as the molar mass reduction after extrusion was 51 %, resulting in less chain entanglements and therefore a lower modulus. Here, we can conclude that the crystallinity and the molar mass have an opposing influence on the tensile modulus. The filament obtained exploiting the final optimized parameters of 270 °C and 3' showed the highest modulus within its series (i.e. 1.28 ± 0.22 GPa) and a drastic increase in the ultimate tensile strain (i.e. 219.01 ± 122.44 %), which confirmed the optimal processing settings resulting in the lowest crystallinity degree and molar mass reduction. When analyzing the ultimate tensile strength and strain results of the filaments processed on lab-scale, a large deviation was noticed, which is the result of the uneven filament diameter. Therefore, those filaments were excluded from further processing, more specifically FFF. All filaments showed a lower tensile modulus compared to the benchmark

Table 5
Overview of the SEC results of $rPET_p$ and the extruded rPET filaments with a filament diameter of 1.75 and 2.85 mm processed with an industrial-scale extruder and the degree of crystallinity (X_c) obtained via mDSC.

	M_n [g/mol]	M_w [g/mol]	$Đ$	X_c [%]
$rPET_p$	7500	21400	2.9	36.3
$rPET_{1.75\ mm}$	7300	14300	2.0	11.8
$rPET_{2.85\ mm}$	8500	16600	2.0	15.8

Table 6
Overview of the tensile modulus (E), ultimate tensile strength (σ_u) and strain (ε_u) of the benchmark materials $vPET_f$ and $rPET_f$ and the filaments extruded on lab and industrial scale tested in tensile mode (n = 7).

	E [GPa]	σ_u [MPa]	ε_u [%]
$vPET_f$	1.49 ± 0.12	44.91 ± 2.64	420.01 ± 45.29
$rPET_f$	1.63 ± 0.05	45.88 ± 1.79	446.51 ± 31.21
$rPET_{275\ °C,\ 5'}$	1.05 ± 0.16	32.83 ± 8.54	5.63 ± 3.65
$rPET_{275\ °C,\ 3'}$	0.94 ± 0.07	43.14 ± 10.39	40.42 ± 22.49
$rPET_{270\ °C,\ 5'}$	0.98 ± 0.15	46.43 ± 9.29	28.50 ± 16.39
$rPET_{270\ °C,\ 3',\ ice}$	1.28 ± 0.22	39.6 ± 3.91	219.01 ± 122.44
$rPET_{1.75\ mm}$	1.53 ± 0.19	45.49 ± 2.95	362.33 ± 15.31
$rPET_{2.85\ mm}$	1.47 ± 0.08	43.31 ± 2.74	408.01 ± 60.62

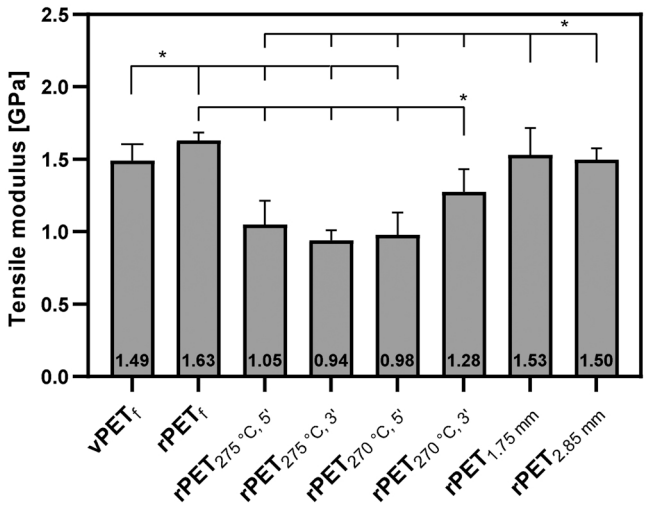

Fig. 2. Overview of the tensile modulus of the benchmark materials $vPET_f$ and $rPET_f$ and the filaments extruded on lab and industrial scale. Significant differences ($p < 0.05$) are denoted with an asterisk (*).

$vPET_f$ and $rPET_f$, except for the filaments extruded on the lab-scale extruder with the optimized parameters and the filaments on the industrial-scale extruder. The tensile moduli of $rPET_{1.75\ mm}$ and $rPET_{2.85\ mm}$ were not significantly different, indicating that mechanical properties remained identical when the diameter is varied during extrusion on the industrial-scale extruder. Moreover, it can be concluded that the recycling process does not impact the tensile modulus and ultimate tensile strength of the filaments when produced on an industrial scale as there was no significant difference found between the commercial recycled and non-recycled filaments. Lastly, also the ultimate tensile strain showed superior results when compared with the filaments processed on lab-scale. It is therefore concluded that when using the optimized extrusion parameters, the mechanical properties of recycled PET are not inferior to commercial virgin and recycled PET filaments.

3.3. Fused filament fabrication with PET

Multiple factors have been described in literature to act on the mechanical properties of FFF printed parts. The factors that affect resulting tensile modulus and strength are polymer degradation, the degree of crystallinity, the printing process parameters (i.e. printing temperature and build plate temperature), the level of interlayer diffusion and void fraction.[52–55] This section focuses on these factors and how they affect the mechanical performance of the printed rPET, compared to printed vPET. Firstly, only the Ultimaker 3, requiring filaments with a diameter of 2.85 mm, was used to investigate the influence of the different printing parameters. Afterwards, also the Prusa i3 MK3S, requiring filaments with a diameter of only 1.75 mm, was used as FFF printer mainly to investigate the intrinsic characteristics.

3.3.1. Effect of printing temperature

As evidenced for PEEK, identifying the optimum printing temperature for a semi-crystalline material requires thorough investigation due to its crystallization behavior.[20] Therefore, the influence of the printing temperature was investigated using commercial $rPET_f$. Via mDSC, it was observed that $T_{m,1}$ of $rPET_p$ was ± 240 °C, while $T_{m,2}$ was ± 250 °C. Therefore, 240 °C was initially selected for printing. However, the material obstructed the nozzle quickly due to fast solidification.[56] Hereafter, higher printing temperatures were selected and evaluated, namely 250, 260 and 275 °C. When the highest temperature from this range was used, printing was possible, although the viscosity was too low resulting in over-extrusion and therefore incorrect shape fidelity and lowered print accuracy. Moreover, one of the reasons for polymer degradation during filament extrusion in Section 3.2.1. was the use of an extrusion temperature of 275 °C. Both 250 and 260 °C as printing temperature did not give raise to nozzle blocking nor to over-extrusion, but keeping the temperature to a minimum is beneficial for the polymer degradation and print accuracy. Besides polymer degradation, Ahn *et al.* showed that a nozzle temperature of 270 or 280 °C during printing of ABS only had a little effect on the mechanical properties.[57] The results showed that 250 °C was the optimal printing temperature for $rPET_f$ since the latter resulted in the lowest polymer degradation while the mechanical properties were not affected. Hence, this printing temperature was subsequently used throughout the course of the experiments. For both $vPET_f$ and $rPET_{2.85\ mm}$, the same temperature could be used to obtain prints with high accuracy which confirms that recycling does not have an influence on the filament properties nor on the optimal printing temperature (see Table S1, Supporting information).

3.3.2. Effect of build plate temperature on shrinkage and mechanical properties

Next to the printing temperature, also the effect of the build plate temperature on the crystallinity and mechanical properties of the printed parts was investigated. It is known from literature that shrinkage and warpage can occur for certain materials (i.e. ABS and PP) if the build plate temperature is too low.[25,26,58] This is the result of thermal contraction occurring during material extrusion, due to the large thermal gradient, resulting from fast cooling.

As PET is semi-crystalline and has a high degree of crystallinity (30 – 50 %), potential shrinkage needs to be considered, as already evidenced by Chatham *et al.*[19] Therefore, pressure-volume-temperature-measurements (pvT) were performed, which resulted in plots representing the specific volume change during cooling at a constant rate while the pressure is fixed. Herein, $vPET_f$, $rPET_f$, $rPET_p$ and $rPET_{2.85\ mm}$ were cooled starting from 290 °C. The results in Fig. 3 show that the specific volume decreases linearly until the crystallization temperature T_c of the material, which is located at higher temperatures due to the slow cooling rate (i.e. 0.1 °C/s). Hereafter, a large change in specific volume occurred when the temperature was above the T_g because of the formation of dense crystals during crystallization. In total, a relative specific volume decrease of 18 % is obtained when PET is cooled down from 290 °C to 40 °C, of which around 5 % is related to shrinkage due to crystallization and 13 % to thermal expansion. The combination of thermal expansion and crystallization will result in a shrinkage and warpage effect after extrusion. Furthermore, all PET materials including the commercial non-recycled PET and the self-extruded recycled filaments showed a similar behavior and shrinkage value during constant cooling, which confirms the statement that recycled PET possesses the same characteristics as virgin PET. Moreover, the coefficient of thermal expansion (CTE) could be calculated for all materials in the range of 40–50 °C as shown in Table S2 and it is concluded that the CTE values are in agreement with literature which performed thermal expansion measurements of virgin PET.[28,59] Spörk *et al.* (2018) performed the same analysis with semi-crystalline PP and compared with amorphous ABS.[60] As in both cases the relative specific volume was plotted, the PET results could be compared with PP and ABS. The PET results show the same trend as PP, involving a drastic volume change during crystallization, while the specific volume of ABS decreased linearly until its T_g (i.e. 110 °C) and showed over the whole temperature range smaller volume changes. Although ABS also imparts a change in specific volume, shrinkage is mostly resolved by increasing the build plate temperature slightly above its T_g which reduces the surface tension between the build plate and the ABS and increases the contact area.[58] To investigate the impact of the build plate temperature on the shrinkage of printed rPET parts, the latter was investigated here as well.

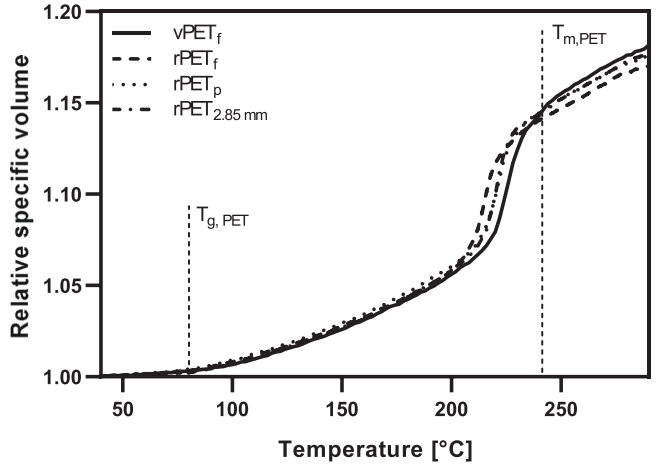

Fig. 3. Schematic overview of the pvT analyses on the benchmarked materials $vPET_f$ and $rPET_f$, compared with $rPET_p$ and $rPET_{2.85\ mm}$.

Although AM with virgin PET has already been reported in literature, the occurrence of warpage and shrinkage of both vPET and rPET has not been studied yet.[18,27] However, small changes in the printing process can already have a large impact. Herein, a low and a high build plate temperature were selected, respectively 40 °C versus 100 °C to print with $rPET_f$. The latter temperature was selected as this was higher than the T_g of PET (80 °C) and the maximum temperature the build plate could reach. It was successful to print a rectangular part in both cases, although the part often detached from the printing plate when the low temperature of 40 °C was used. This could be explained by an insufficient first layer adhesion to the plate because of the decrease in free volume during cooling. In case of applying a temperature of 100 °C, the temperature was above the T_g and therefore the chain mobility of PET was higher, which resulted in an enhanced adhesion. The latter has already been described previously for multiple other amorphous and semi-crystalline materials.[58] When the print job was finished when 100 °C was used, the build plate temperature decreased to room temperature and the printed part detached automatically from the glass surface.

In order to reduce shrinkage, various options exist with the addition of fillers to fill up the free volume being the most common one.[61–63] Examples of fillers include carbon fibers, glass fibers and cellulose. Another option to reduce shrinkage during cooling is via reducing the specific volume change, which can be realized by polymer modification to reduce the crystallinity.[62] Amongst others, the tacticity or side chain length and thus the density can be altered or copolymers could be synthesized. Furthermore, blending with other (amorphous) polymers is also an option.[64].

The influence of the build plate temperature on the mechanical properties of the materials was determined by comparing the tensile modulus of the rectangular parts printed at temperatures of 40 versus 100 °C with $rPET_f$. All other printing and material parameters were kept constant, including the optimized printing temperature of 250 °C and the tracks printed perpendicular to the loading direction during tensile testing. It was found that the $rPET_f$ parts printed using a build plate temperature of 100 °C showed no significant difference in tensile

modulus compared with the parts printed using a build plate temperature of 40 °C, respectively 2.17 ± 0.02 GPa and 2.05 ± 0.21 GPa. The tensile modulus resulting from a build plate temperature of 40 °C showed rather high scattering that could be caused by shrinkage. Raising the build plate temperature above the T_g of the polymer thus had no influence on the tensile modulus of the printed parts. Notwithstanding the fact that increasing the build plate temperature does not result in superior mechanical properties, exploiting a higher temperature is useful to avoid shrinkage of the printed parts. In order to verify this hypothesis, parts were printed using a build plate temperature of 100 °C with the non-recycled $vPET_f$ and extruded recycled $rPET_{2.85\ mm}$. Prints with high accuracy and without any sign of shrinkage were obtained and therefore, it can be concluded that the same printing parameters for recycled and non-recycled PET could be used without influencing the final result.

3.3.3. Effect of cooling on the crystallinity and mechanical properties

The printing conditions including fan cooling, nozzle and build plate temperatures were altered to investigate their influence on the crystallinity and mechanical properties of the printed parts. As already reflected by the variations of the degree of crystallinity during extrusion and shrinkage controlled by the build plate temperature, cooling is an important parameter influencing the semi-crystallinity of PET. If the printed material is cooled down quickly, the degree of crystallinity will be lower, which will result in a semi-crystalline material with more amorphous parts and therefore different mechanical properties (e.g. reduced tensile modulus).[65–67] On the other hand, a slower cooling will result in a higher degree of crystallinity and therefore an improved modulus. [65–67] On the other hand, a slower cooling will result in a higher degree of crystallinity and therefore an improved modulus. Therefore, in this study, the fan cooling and temperatures during 3D printing of $rPET_f$ were varied and thereafter, the mechanical properties were assessed. The fan cooling was activated when an amorphous part was targeted. To cool down even more quickly, the build plate temperature was set at 40 °C, while the printing temperature was 250 °C. As a result, the printed parts showed a transparent color which already indicated a low degree of crystallinity (see Fig. S7a, Supporting information).[24] On the other hand, to obtain a stiffer material, no fan cooling was applied and the build plate and printing temperature were respectively 100 and 275 °C, resulting in a higher crystallinity as reflected by the opaque nature of the part (see Fig. S7b, Supporting information). Via mDSC, the thermal properties and the degree of crystallinity were determined (see Table 7).

Via tensile testing, the tensile moduli of the rectangular parts were determined and indeed, the modulus was significantly higher when the cooling was omitted. Moreover, $rPET_{cooled}$ exhibited a ductile fracture during the plastic elongation, while $rPET_{not\text{-}cooled}$ showed brittle behavior (see Fig. S8, Supporting information). This is in agreement with the degree of crystallinity and its influence on the modulus. The degree of crystallinity of $rPET_{cooled}$ was 1.4 %, resulting in an almost complete amorphous printed part and tensile modulus of 1.59 ± 0.1 GPa, while $rPET_{not\text{-}cooled}$ was more semi-crystalline with a degree of crystallinity of 21.2 % and resulted in a modulus of 1.83 ± 0.09 GPa.

3.3.4. Effect of printing direction on mechanical properties

As the mechanical performance of parts printed via FFF are highly dependent on the printing direction, the tensile properties of printed $rPET_f$ parts were investigated along two different printing directions, namely 0° and 90°.[54] The 0° samples were printed in such a way that the tracks were parallel to the loading direction, as shown in Fig. 4a, and is further referred to as [0°]. The 90° samples were printed with the tracks perpendicular to the load, as shown in Fig. 4b and c, and is further referred to as [90°].

Besides printing orientation, also build orientation affects the mechanical performance, via the interlayer properties. Because FFF printed parts are known to suffer from weak interfacial bonds between tracks, the cohesion between adjacent tracks was investigated. The degree of bonding between adjacent tracks is dependent on the joining process along the partially melted polymer-polymer interface, as described earlier in literature.[68–70] A high level of molecular interdiffusion at the interface, and hence mechanical interlocking between tracks, is preferred, as this leads to a higher level of load transfer and improved mechanical performance. The [90°] lay-up was printed in two different ways, in-plane and out-of-plane with respect to the build plate. Aiming to test the cohesion between adjacent tracks within one layer (intra--layer bond strength), one series of the [90°] lay-up was printed in-plane, horizontally on the built plate, see Fig. 5b.[57,71,72] A second series of the [90°] lay-up was printed out-of-plane, upright on the build plate, allowing to test the cohesion between successive layers (inter-layer bond strength) (see Fig. 5c). The two approaches are respectively referred to as [90°]-INTRA and [90°]-INTER. The tensile strength was taken as a measure for the cohesion between the tracks. Furthermore, the optimized printing settings were used, including a printing temperature of 250 °C while the build plate temperature was 100 °C to avoid shrinkage during printing.

3.3.4.1. Effect of varying printing direction on mechanical properties. To investigate the influence of the printing direction on the void fraction and mechanical properties, $rPET_f$ samples were printed in the [0°] and [90°]-INTRA direction. The type of voids and the void fraction were determined via optical microscopy of polished cross-sections of the printed samples. Two types of voids were identified, namely intra-track voids located inside the tracks and inter-track voids located between tracks, either within one layer or between layers. The intra-track voids were most likely gaseous pores which were formed during extrusion of the filaments.[73] Only a few intra-track voids were found, which were mostly circular and in the range of 10–20 μm in diameter. The inter-track voids on the other hand are the gaps between tracks generated during printing, and depend on nozzle size and shape, melt flow characteristics, printing direction, and thermodynamic parameters, like cooling rate and nozzle and build plate temperatures.[74] The inter-track void fraction and maximal void size are summarized in Table 8. Microscopy images showing the inter-track voids in the [0°] and [90°]-INTRA samples are presented in Fig. 5. A gradual increase in void content can be observed from the bottom layers up to the upper layers. This phenomenon can be ascribed to the annealing effect of the heated build plate that keeps the layers in close proximity to the build plate at a higher temperature throughout the printing process. The thermal gradient caused by the heated build plate has been described before in literature.[75] It can be concluded that the void content as well as the void shapes for [0°] and [90°]-INTRA are similar. Compared with literature for parts printed with other commonly used filaments, the measured void content is low. For example for PLA, a void content of around 16 % has been reported for a multidirectional layup.[74] For densely packed aligned ABS, a minimum void density of 6.8 % was found earlier.[76] For PA6, a void fraction of 0.07 % and 0.10 % were found depending on the build orientation.[77].

A significant difference ($p < 0.05$) between the tensile modulus of [0°] and [90°]-INTRA was found, with a modulus of 2.65 ± 0.14 GPa for parts printed in the [0°] direction and 2.17 ± 0.02 GPa for parts in the [90°]-INTRA direction (see Table 9 and Fig. 6). In conclusion, the modulus of the [0°] parts was 22.1 % higher than of the [90°]-INTRA,

Table 7
Thermal properties of both $rPET_{cooled}$ and $rPET_{not\text{-}cooled}$ printed parts, including the degree of crystallinity (Xc) measured with mDSC.

	T_g [°C]	T_{cc} [°C]	$T_{m,1}$ [°C]	$T_{m,2}$ [°C]	T_c [°C]	X_c [%]
$rPET_{cooled}$	82	113	241	250	198	1.4
$rPET_{not\text{-}cooled}$	81	107	243	251	204	21.2

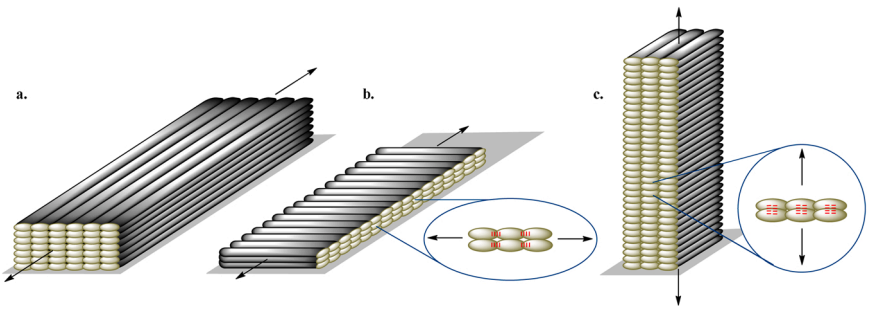

Fig. 4. Schematic representation of the different printing directions that were investigated, showing a. the in-plane [0°] lay-up, b. the in-plane [90°]-INTRA which is printed horizontally on the build plate, and c. the out-of-plane [90°]-INTER lay-up which is printed upright on the build plate.

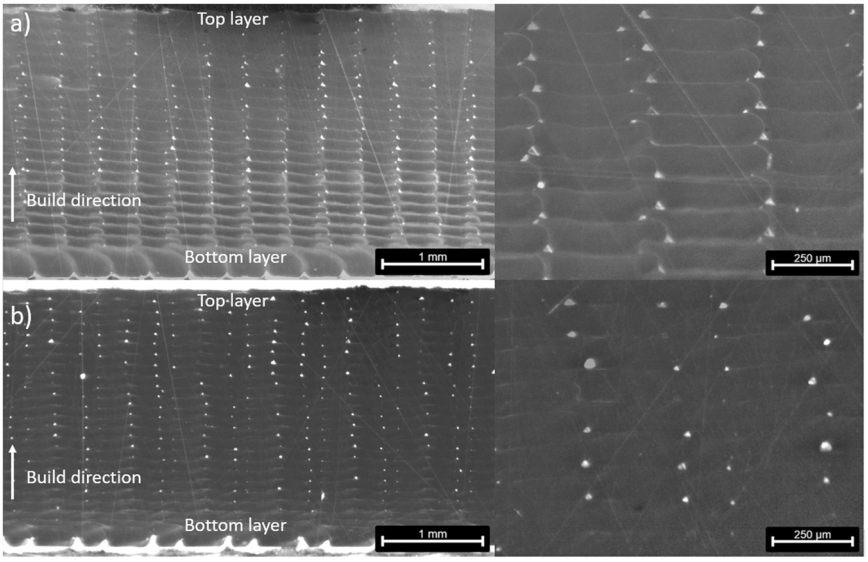

Fig. 5. Micrographs showing the void content and void geometry of a) $rPET_f$ printed in [0°] with 2.85 mm filament and b) $rPET_f$ printed in [90°]-INTRA. The entire thickness of the sample is visualized in the images on the left. The build direction is shown with an arrow. Top and bottom layers are indicated.

Table 8
Inter-track void contents of the tested tensile samples and maximal void size.

Filament	Filament diameter [mm]	Orientation	Void fraction [%]	Maximal void size [µm]
$vPET_f$	2.85	[0°]	0.03	40
$rPET_f$	1.75	[0°]	0.85	58
	2.85	[0°]	0.84	49
	2.85	[90°]-INTRA	0.70	62
	2.85	[90°]-INTER	2.71	117
$rPET_{2.85\ mm}$	2.85	[0°]	0.29	38

Table 9
Overview of the tensile modulus (E) of all samples printed with the commercial $vPET_f$ and $rPET_f$ and the self-extruded $rPET_{2.85\ mm}$ while the filament diameter ($ø_{filament}$) and orientation varied. The effective modulus (E^{eff}) has been calculated to correct for the void content.

Filament	$Ø_{filament}$ [mm]	Orientation	E [GPa]	E^{eff} [GPa]
$vPET_f$	2.85	[0°]	2.51 ± 0.16	2.58
$rPET_f$	1.75	[0°]	2.41 ± 0.04	2.43
	2.85	[0°]	2.65 ± 0.14	2.67
	2.85	[90°]-INTRA	2.17 ± 0.02	–
	2.85	[90°]-INTER	1.82 ± 0.28	–
$rPET_{2.85\ mm}$	2.85	[0°]	2.37 ± 0.08	2.38

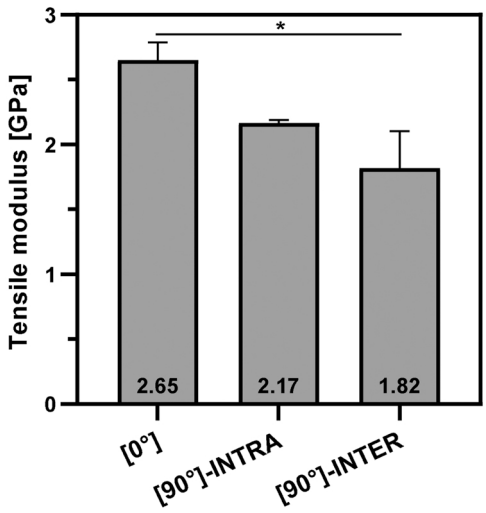

Fig. 6. Schematic overview of the tensile modulus of $rPET_f$ printed parts in different printing directions, namely [0°], [90°]-INTRA and [90°]-INTER obtained via tensile testing. Significant differences ($p < 0.05$) are denoted with an asterisk (*).

proving that the printed part is anisotropic. One explanation of the significantly higher modulus of the [0°] parts compared with the [90°]-INTRA parts could be the difference in the orientation of the printed filaments. The shear stress imposed on the melt during extrusion through the heated nozzle aligns the polymer chains inside the track to a certain degree.[20,78] Therefore, the tensile modulus of the [0°] samples is expected to depend on the polymer chains that were aligned along the loading direction. Conversely, the polymer chains in the printed filaments of the [90°]-INTRA sample were oriented perpendicular to the load. Consequently, the modulus of the [90°] samples is expected to depend on the transverse properties of the polymer. It is however possible that the macromolecular alignment that is induced by the extrusion relaxes after deposition. The orientation can disappear if the polymer chains gain sufficient mobility due to the heat of the build plate or the time on the build plate.[24] But if the alignment of the polymer chains is retained, it is proven to improve the tensile modulus.[79,80] However, since the [90°] sample is effectively a composite of bulk polymer and weld lines for which the characteristics depend on the extent of macromolecular interdiffusion, it is difficult to propose an exact explanation for the lower modulus. The cross-sections that were used in the calculation of the tensile modulus of the 0° samples, listed in Table 9, could be corrected to account for the void content. As the void content was quite small (<1 %), the effective tensile modulus was not substantially different from the tensile modulus that was calculated without a void correction (see Table 9). The tensile modulus of the [90°] samples could not be corrected for the void content as the polished cross-section of the sample would not be representative of the fracture surface.

Recently, the anisotropy and the effect of printing direction of various semi-crystalline materials via FFF have been published, including PETG, PLA, PP and PA.[77,81–83] A tensile modulus of 2.05 GPa and 1.89 GPa for PETG printed in the 0° and 90° direction respectively was reported, indicating a drop of 7.8 %.[81] For 90° PLA samples, a decrease of 7.4 % was shown compared to 0° PLA samples.[83] For PA the opposite was found, a higher modulus in the 90° printing direction, more specifically 10.4 % higher compared with 0° samples.[73] Moreover, a tensile modulus of 2.11 ± 0.20 GPa was found for rPET printed in a ± 45° orientation with a nozzle temperature of 270 °C and a build plate temperature of 30 °C.[18].

3.3.4.2. Effect of build orientation on cohesion between tracks. To examine the effect of the build orientation, samples were printed via [90°]-INTRA and [90°]-INTER direction using $rPET_f$. Inter-track voids were visualized via optical microscopy images of polished cross-sections of the printed samples, see Fig. 5b and Fig. 7. The microscopy images show that the polished samples from [90°]-INTRA and [90°]-INTER printed parts contained two inter-track void geometries, including circular for smaller voids (i.e. 20 μm) and triangular voids in case of larger entities (i.e. > 20 μm). Furthermore, it is noticed that the inter-track voids of [90°]-INTER are larger and more abundant when compared to the voids of the cross-section of [90°]-INTRA (see Table 8). A possible explanation for this phenomenon is that the majority of the [90°]-INTER sample is deposited at a larger distance from the heated build plate. The [90°]-INTRA sample, however, is printed closer to the heated build plate, remaining at high temperature for a longer time. It is hypothesized that the larger voids for [90°]-INTRA printed samples will largely influence the failure properties as voids can concentrate stress, leading to failure of the sample.

To investigate the effect of build orientation on the bond between the tracks, the tensile strength was measured for [90°]-INTRA and [90°]-INTER as the intra-layer strength is smaller than the tensile strength of the bulk polymer.[72] Table 9 shows the tensile modulus, ultimate tensile strength and strain of the samples. The [90°]-INTER parts showed a significant decrease of 70 % in tensile strength (11.9 ± 0.6 MPa) compared with the [90°]-INTRA parts (39.3 ± 2.9 MPa). The large difference shows that the bond quality or cohesion between subsequently printed layers is lower than the cohesion between adjacent tracks within one layer, proving anisotropy due to the building orientation. The [90°]-INTRA parts stayed at a higher temperature throughout the printing process compared with the [90°]-INTER parts, thanks to their proximity to the heated build plate. The heated build plate induces a higher crystallization rate and crystalline content, resulting in a higher tensile modulus.[79] Furthermore, keeping the substrate at a high temperature is important to achieve high interfacial bonding and consequently higher load bearing capacities.[21] An increased build plate temperature hence improves both modulus and

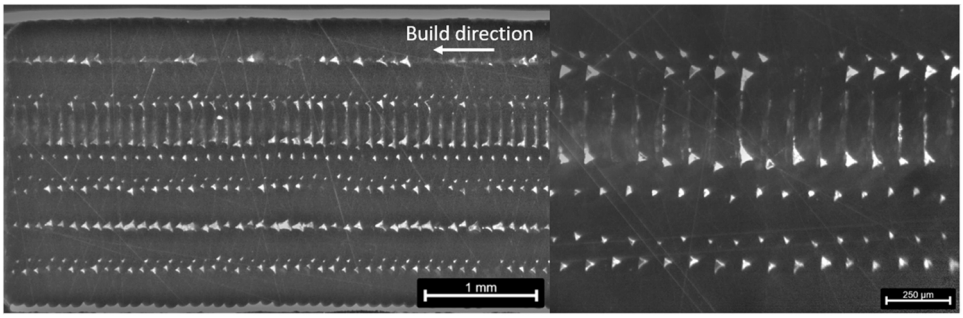

Fig. 7. Micrograph showing the void content and void geometry of $rPET_f$ printed in [90°]-INTER. The entire thickness of the sample is visualized in the image on the left. The build direction is shown with an arrow.

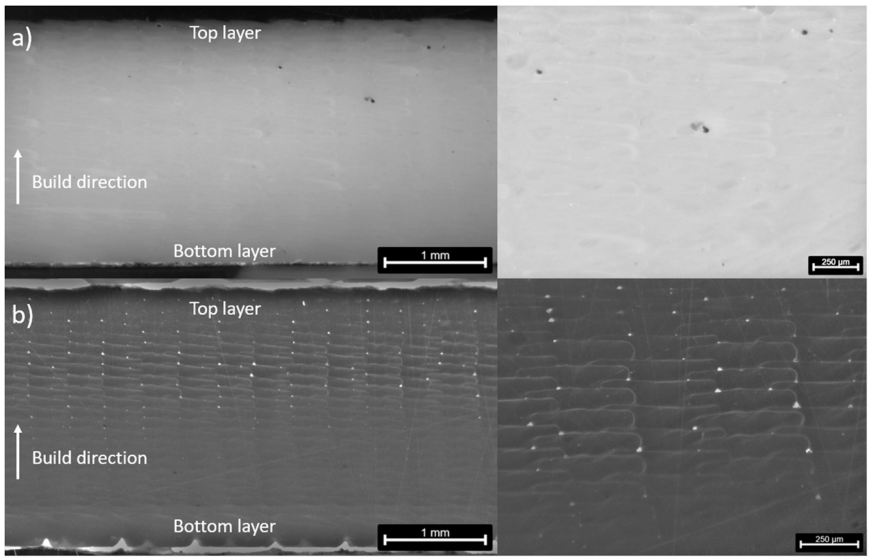

Fig. 8. Micrographs showing the void content and void geometry of a) $vPET_f$ and b) $rPET_{2.85\ mm}$. The entire thickness of the sample is visualized in the images on the left. The build direction is shown with an arrow. The top and bottom layers are indicated.

strength.[53] The lower strength of the [90°]-INTER parts suggests that the contact temperature of the deposited tracks with the substrate was too low to promote interdiffusion with adjacent tracks. This resulted in a higher void fraction and void size for [90°]-INTER compared with [90°]-INTRA (see Table 8).

3.3.5. *Properties of printed rPET parts against commercial benchmark materials*

To assess the effects of the filament extrusion on mechanical properties, parts were printed using $rPET_{2.85\ mm}$ filament extruded from commercial $rPET_p$ pellets and were compared with parts printed with commercial $vPET_f$ filament and $rPET_f$. All printing parameters were the same (i.e. printing temperature of 250 °C and a build plate temperature of 100 °C), while a printing direction of [0 °] was maintained.

The print quality was examined via optical microscopy of polished cross-sections of the printed samples (see Fig. 5a and Fig. 8). Multiple differences between the samples were observed. Firstly, almost no inter-track voids were observed in the $vPET_f$ samples indicating a better cohesion between the tracks. This could be the result of better flow properties, higher heat capacity or better heat transfer between printed tracks. Moreover, the annealing effect induced by the heated build plate was more present in $rPET_{2.85\ mm}$ than in $rPET_f$, as voids were almost absent in the first layers of $rPET_{2.85\ mm}$.[84] The amount and size of voids increased in the upper layers of $rPET_{2.85\ mm}$, with a maximum void size of 38 µm and a total void fraction of only 0.29 %. It is concluded that $rPET_f$ included the most voids, however, the void fractions remain low (< 1 %).

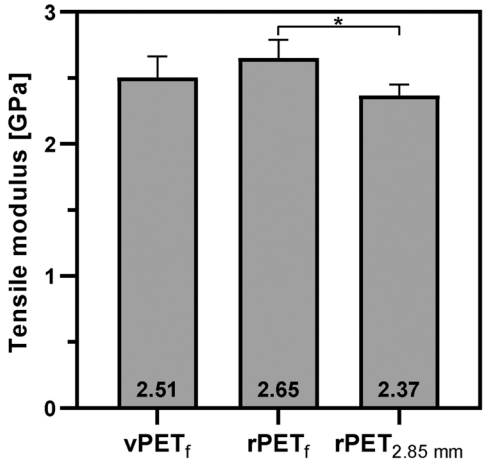

Fig. 9. Schematic overview of the tensile modulus of $vPET_f$, $rPET_f$ and $rPET_{2.85\ mm}$ printed parts obtained via tensile testing. Significant difference ($p < 0.05$) is denoted with an asterisk (*).

Tensile testing on the printed samples showed no significant difference in moduli between the $rPET_f$ and $vPET_f$ printed parts, thereby proving that the recycling process of commercial PET had no negative influence on the tensile modulus of the printed parts (see Table 9 and Fig. 9). The extrusion of the pellets however, did affect the tensile modulus of the printed parts. More specifically, the tensile modulus of parts printed with the commercial $rPET_f$ filament was 12 % higher than the tensile modulus of parts printed with $rPET_{2.85\ mm}$ which was herein extruded from $rPET_p$. This small difference can be explained by the lower molar mass of $rPET_{2.85\ mm}$ compared with $rPET_f$, respectively 16600 and 21000 g/mol. Together with polymer degradation, also the crystallinity of the parts printed with $rPET_{2.85\ mm}$ was slightly lower, namely 27.8 %, while the values for the printed $vPET_f$ and $rPET_f$ parts were respectively 31.9 % and 31.3 %. It is hypothesized that the small difference in crystallinity will not have a pronounced influence on the tensile modulus. Moreover, the molar mass of $vPET_f$ was 18000 g/mol, which is ranging between the values of $rPET_{2.85\ mm}$ and $rPET_f$. It can be concluded that the molar mass plays an important role in the 3D printing process and will influence the mechanical properties of the printed parts. Besides the molar mass, Table 8 showed that the void fractions of the three printed samples were very low with values below 1 %. Therefore, the calculated tensile modulus was barely affected by a void-correction. Furthermore, the recycling of PET does not have a negative impact on the mechanical properties and printing accuracy as the tensile modulus of $rPET_f$ and $rPET_{2.85\ mm}$ was not significantly different from $vPET_f$.

In Fig. 10, the fracture surfaces of $vPET_f$, $rPET_f$ and $rPET_{2.85\ mm}$ obtained via scanning electron microscopy (SEM) are shown in order to inspect the layer adhesion and the presence of voids after fracture via tensile testing. When the fracture surfaces are compared, the failure mode varies depending on which material is used. While $vPET_f$ shows a stepped-like fracture, $rPET_f$ and $rPET_{2.85\ mm}$ exhibit a smooth failure at one height. More pronounced weld lines between the printed layers are detected for $vPET_f$, indicating that the inter-layer cohesion might be lower compared to $rPET_f$ and $rPET_{2.85\ mm}$. Besides the weld lines

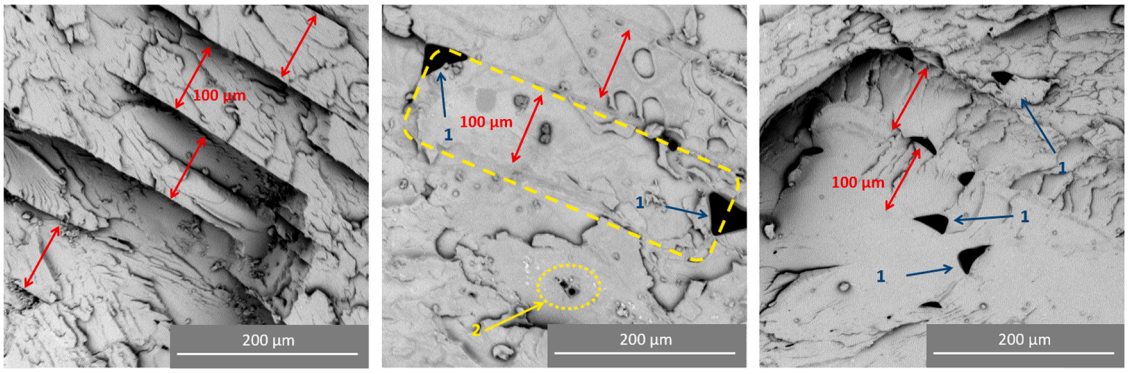

Fig. 10. SEM images showing the fracture surface of $vPET_f$ (a.), $rPET_f$ (b.) and $rPET_{2.85\ mm}$ (c.). The printed layers could be identified and are indicated with red arrows, while voids are indicated with a blue arrow.

between the layers, the weld lines between the printed tracks are completely absent. This finding validates that the nozzle temperature of 250 °C was high enough to enable a high level of diffusion at the interface. The SEM images of the fractured surfaces verify that $vPET_f$ does not include voids, while $rPET_f$ and $rPET_{2.85\ mm}$ do show larger inter-layer voids and smaller intra-track voids.[74] Although the inter-layer voids are present on the SEM images, this was not the case for the whole cross-section of both prints. The voids from $rPET_f$ measure approximately 44 µm, while the voids from $rPET_{2.85\ mm}$ measure 30 µm. Moreover, the triangular shape of the inter-layer voids is preserved after fracture. It can be noticed that the fracture of these printed parts proceeded at one height, while weld lines between layers or tracks are absent.

3.3.6. *Effect of printer characteristics on crystallinity and mechanical properties*

The influence of the printer's intrinsic characteristics was examined by comparing the void fraction and mechanical properties of $rPET_f$ parts printed on the Ultimaker 3 and the Prusa i3 MK3S in the [0 °] direction. To generate the G-code, the same slicer was used to avoid different algorithms. All printing parameters were kept constant, although the printing temperature of the Prusa i3 was 10 °C higher as printing at 250 °C obstructed the nozzle. The nozzle was blocked irrespective of using $rPET_f$ or $vPET_f$ as the material did not melt due to a different printhead setup. The build plate temperature was 100 °C to avoid shrinkage during printing. Moreover, the filament diameter was different as the filament diameter for the Ultimaker 3 was 2.85 mm, while the Prusa i3 required filaments with a diameter of 1.75 mm.

The void content was analyzed via polished cross-sections of the printed samples and are shown in Fig. 11. Although the inter-track void content of the samples printed on the Prusa and Ultimaker is similar, the voids in the Prusa samples are smaller and more uniformly distributed over the thickness. The annealing effect of the build plate was observed in the Ultimaker samples, but not in the Prusa samples. These observations are probably the effect of the different cooling characteristics of the Prusa and Ultimaker printers. Intra-track voids were present in both, as they do not depend on printer properties but are created in the extrusion process. These voids were few, circular and 20–60 µm in diameter.

Via tensile testing, it was found that there was a significant difference ($p < 0.05$) in tensile modulus between the Ultimaker (i.e. 2.65 ± 0.14 GPa) and Prusa (2.41 ± 0.04 GPa) printed parts (see Table 9). The latter can be explained by the degree of crystallinity, which is higher for the parts printed with the Ultimaker (i.e. 31.3 %) as compared to those obtained from the Prusa (i.e. 10.6 %). It was already proven before that cooling had a major impact on the crystallinity and therefore its mechanical properties (vide supra). Here, it is hypothesized that the fan cooling of the Prusa cools more during and after printing, which results in a sample with less crystalline parts. Ferrari *et al.* have suggested that the degree of crystallinity is the most relevant factor controlling mechanical properties, as tensile modulus and strength increase, and failure strain decreases with an increasing degree of crystallinity.[27] Despite the difference in fan cooling, both printers were perfectly able to print with rPET filaments by using the parameters investigated in this study.

4. Conclusion

The present work focused on the processing of recycled PET towards filaments via extrusion and using those as feedstock for fused filament fabrication. The extrusion parameters were optimized and the obtained filaments were compared with commercial virgin and recycled PET filaments. The results showed that polymer degradation occurred depending on the residence time in the extruder. Moreover, the degree of crystallinity of the filaments was affected by the extrusion conditions and influenced the mechanical properties. The printing parameters for FFF were optimized towards a printing temperature of 250 °C for

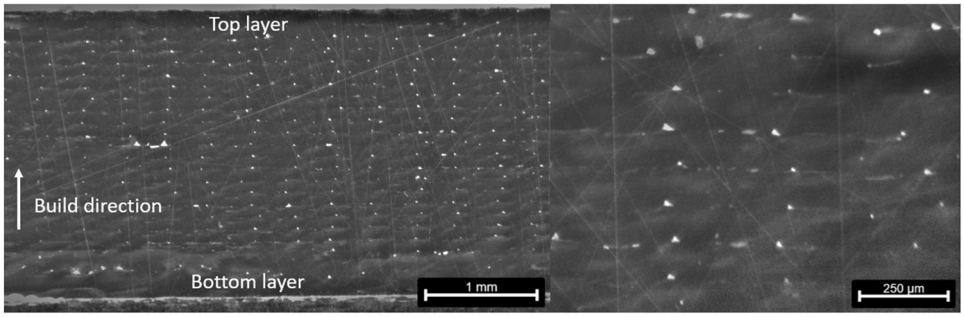

Fig. 11. Micrographs showing the void content and void geometry of $rPET_f$ printed in [0°] with 1.75 mm filament. The entire thickness of the sample is visualized in the image on the left. The build direction is shown with an arrow. The top and bottom layers are indicated.

Ultimaker 3 and 260 °C for Prusa i3 MK3S and a build plate temperature above the T_g. Furthermore, it was shown that fan cooling and the combination of printing and build plate temperature had a large impact on the degree of crystallinity and therefore on the mechanical properties of the printed parts. The printing direction was varied between parallel and perpendicular to the tensile load. The printed parts were anisotropic in terms of tensile modulus. Lastly, also the used FFF printer influenced the printed outcome as its characteristics such as fan cooling could slightly differ. This study has shown that prolonging the lifecycle of PET by remanufacturing PET-waste into rPET filaments for FFF 3D printing is possible and therefore interesting from a sustainability point of view. When using optimized extrusion and printing parameters, rPET filaments have the potential to be used in a wide range of 3D printing applications including automotive and other fields in which vPET is currently applied as the use of rPET filaments does not have a negative impact on the mechanical properties and print accuracy.

CRediT authorship contribution statement

Babs Van de Voorde: Investigation, Conceptualization, Writing – original draft, Writing – review & editing, Data curation, Formal analysis, Visualization, Methodology, Validation, Software. **Amalia Katalagarianakis:** Investigation, Conceptualization, Writing – original draft, Writing – review & editing, Data curation, Formal analysis, Visualization, Methodology, Validation, Software. **Sofie Huysman:** Resources, Validation. **Antoniya Toncheva:** Formal analysis, Resources. **Jean-Marie Raquez**: Resources, Validation. **Ivica Duretek:** Data curation, Resources, Validation. **Clemens Holzer:** Resources, Validation. **Ludwig Cardon:** Resources, Writing – review & editing, Validation. **Katrien V. Bernaerts:** Data curation, Resources, Validation. **Danny Van Hemelrijck:** Supervision, Funding acquisition, Writing – review & editing, Validation. **Lincy Pyl:** Supervision, Funding acquisition, Conceptualization, Writing – review & editing, Validation, Project administration. **Sandra Van Vlierberghe:** Supervision, Funding acquisition, Conceptualization, Writing – review & editing, Validation, Project administration.

Declaration of Competing Interest

The authors declare that they have no known competing financial interests or personal relationships that could have appeared to influence the work reported in this paper.

Acknowledgement

The authors acknowledge the support of the Agency for Innovation and Entrepreneurship Flanders via the Strategic Initiative Materials in Flanders in the framework of the SIM-SBO RELFICOM project, running in the NANOFORCE program.

Appendix A. Supporting information

Supplementary data associated with this article can be found in the online version at doi:10.1016/j.addma.2021.102518.

References

[1] Plastics – the Facts 2020 An analysis of European plastics production, demand and waste data Available online: ⟨https://www.plasticseurope.org/en/resources/publications/4312-plastics-facts-2020⟩ (accessed on Jun 11, 2021).
[2] Ellen MacArthur Foundation, WEF the new plastics economy: rethinking the future of plastics, Ellen. MacArthur Found. (2016) 120.
[3] Mc.Kinsey Center, Ocean conservancy stemming the tide, Land-Based Strateg. a Plast. - Free Ocean (2015) 47.
[4] Archna, V. Moses, S. Sagar, V. Shivraj, S. Chetan, A Review on processing of waste PET (Polyethylene Terephthalate) plastics, Int. J. Polym. Sci. Eng. 1 (2016) 1–13.
[5] J. Scheirs, T.E. Long, Modern Polyesters: Chemistry and Technology of Polyesters and Copolyesters. Modern Polyesters: Chemistry and Technology of Polyesters and Copolyesters, John Wiley and Sons Ltd., 2003, pp. 1–750. ISBN 0471498564.
[6] K.G. Dahmen, N. Maurin, H.A. Richter, C. Mittermayer, Screening of biomedical polymer biocompatibility in NMRI-mice peritoneal cavity. A comparison between ultra-high-molecular-weight polyethylene (UHMW-PE) and polyethyleneterephthalate (PET), J. Mater. Sci. Mater. Med 8 (1997) 239–245.
[7] A. Subramaniam, S. Sethuraman, Biomedical Applications of Nondegradable Polymers. In. Natural and Synthetic Biomedical Polymers, Elsevier Inc,, 2014, pp. 301–308. ISBN 9780123969835.
[8] D.E. Nikles, M.S. Farahat, New motivation for the depolymerization products derived from poly(ethylene terephthalate) (PET) waste: a review, Macromol. Mater. Eng. 290 (2005) 13–30.
[9] F. Awaja, D. Pavel, Recycling of PET, Eur. Polym. J. 41 (2005) 1453–1477.
[10] S.M. Al-Salem, P. Lettieri, J. Baeyens, Recycling and recovery routes of plastic solid waste (PSW): a review, Waste Manag 29 (2009) 2625–2643.
[11] V. Sinha, M.R. Patel, J.V. Patel, PET waste management by chemical recycling: A review, J. Polym. Environ. 18 (2010) 8–25.
[12] N. Torres, J.J. Robin, B. Boutevin, Study of thermal and mechanical properties of virgin and recycled poly (ethylene terephthalate) before and after injection molding, Eur. Polym. J. 36 (2000) 2075–2080.
[13] J.C. Viana, N.M. Alves, J.F. Mano, Morphology and mechanical properties of injection molded poly(ethylene terephthalate), Polym. Eng. Sci. 44 (2004) 2174–2184.
[14] Y. Huang, M.C. Leu, J. Mazumder, A. Donmez, Additive manufacturing: current state, future potential, gaps and needs, and recommendations, in: J. Manuf. Sci. Eng. Trans, 137, ASME,, 2015, pp. 1–11.
[15] J. Gardan, Additive manufacturing technologies: state of the art and trends, Int. J. Prod. Res. 54 (2015) 3118–3132.
[16] S. Chong, G.T. Pan, M. Khalid, T.C.K. Yang, S.T. Hung, C.M. Huang, Physical characterization and pre-assessment of recycled high-density polyethylene as 3D printing material, J. Polym. Environ. 25 (2017) 136–145.
[17] J. Pakkanen, D. Manfredi, P. Minetola, L. Iuliano, About the use of recycled or biodegradable filaments for sustainability of 3D printing: State of the art and research opportunities, in: Proceedings of the Smart Innovation, Systems and Technologies, Vol. 68, Springer Science and Business Media Deutschland GmbH, 2017, pp. 776–785.
[18] N.E. Zander, M. Gillan, R.H. Lambeth, Recycled polyethylene terephthalate as a new FFF feedstock material, Addit. Manuf. 21 (2018) 174–182.
[19] C.A. Chatham, C.E. Zawaski, D.C. Bobbitt, R.B. Moore, T.E. Long, C.B. Williams, Semi-crystalline polymer blends for material extrusion additive manufacturing printability: a case study with poly(ethylene terephthalate) and polypropylene, Macromol. Mater. Eng. 304 (2019) 1–11.
[20] C. Yang, X. Tian, D. Li, Y. Cao, F. Zhao, C. Shi, Influence of thermal processing conditions in 3D printing on the crystallinity and mechanical properties of PEEK material, J. Mater. Process. Technol. 248 (2017) 1–7.
[21] S. Hertle, M. Drexler, Drummer, D. Additive Manufacturing of Poly(propylene) by Means of Melt Extrusion, Macromol. Mater. Eng. 301 (2016) 1482–1493.
[22] S. Ding, B. Zou, P. Wang, H. Ding, Effects of nozzle temperature and building orientation on mechanical properties and microstructure of PEEK and PEI printed by 3D-FDM, Polym. Test. 78 (2019) 1–9.
[23] N.E. Zander, M. Gillan, Z. Burckhard, F. Gardea, Recycled polypropylene blends as novel 3D printing materials, Addit. Manuf. 25 (2019) 122–130.
[24] D. Vaes, P. Van Puyvelde, Semi-crystalline feedstock for filament-based 3D printing of polymers, Prog. Polym. Sci. 118 (2021) 101411.
[25] A.A. Rosli, R.K. Shuib, K.M.K. Ishak, Z.A.A. Hamid, M.K. Abdullah, A. Rusli, Influence of bed temperature on warpage, shrinkage and density of various acrylonitrile butadiene styrene (ABS) parts from fused deposition modelling (FDM), Proc. AIP Conf. Proc. 2267 (2020) 1–10.
[26] C.C. Kuo, Y.R. Wu, M.H. Li, H.W. Wu, Minimizing warpage of ABS prototypes built with low-cost fused deposition modeling machine using developed closed-chamber and optimal process parameters, Int. J. Adv. Manuf. Technol. 101 (2019) 593–602.
[27] F. Ferrari, C.E. Corcione, F. Montagna, A. Maffezzoli, 3D printing of polymer waste for improving people's awareness about marine litter, Polym. (Basel) 12 (2020) 1–14.
[28] M.K.J.E. Exconde, J.A.A. Co, J.Z. Manapat, E.R. Magdaluyo, Materials selection of 3D printing filament and utilization of recycled polyethylene terephthalate (PET) in a redesigned breadboard, Procedia CIRP 84 (2019) 28–32.
[29] Blaine, R.L. *Polymer Heats of Fusion, Therm. Appl. Note*; 109 Lukens Drive, New Castle DE 19720, USA, 2002;
[30] ASTM D3039 / D3039M-17, Standard Test Method for Tensile Properties of Polymer Matrix Composite Materials, Available online: ⟨www.astm.org⟩ (accessed on Jun 11, 2021).
[31] ISO 17744:2004, Plastics — Determination of specific volume as a function of temperature and pressure (pvT diagram) — Piston apparatus method Available online: ⟨https://www.iso.org/standard/33196.html⟩ (accessed on Jun 11, 2021).
[32] K. Weisskopf, Characterization of polyethylene terephthalate by gel permeation chromatography (GPC), J. Polym. Sci. Part A Polym. Chem. 26 (1988) 1919–1935.
[33] O. Olabisi, K. Adewale, Handb. Thermoplast.; Second (2016). ISBN 9781466577237.
[34] F. Welle, Twenty years of PET bottle to bottle recycling - an overview, Resour. Conserv. Recycl. 55 (2011) 865–875.
[35] N. Malik, P. Kumar, S. Shrivastava, S.B. Ghosh, An overview on PET waste recycling for application in packaging, Int. J. Plast. Technol. 21 (2017) 1–24.

[36] S. Venkatachalam, G.N. Shilpa, V.L. Jayprakash, R.G. Prashant, R. Krishna, K. K. Anil, Degradation and recyclability of poly (ethylene terephthalate), Polyester (2012) 75–98.
[37] I.C. McNeill, M. Bounekhel, Thermal degradation studies of terephthalate polyesters: 1, Poly(alkylene terephthalates). Polym. Degrad. Stab. 34 (1991) 187–204.
[38] F. Samperi, C. Puglisi, R. Alicata, G. Montaudo, Thermal degradation of poly (ethylene terephthalate) at the processing temperature, Polym. Degrad. Stab. 83 (2004) 3–10.
[39] B.; Demirel, A.; Yaraş, H. Elçiçek, Crystallization behavior of PET materials, BAÜ Fen. Bil. Enst. Derg. Cilt 13 (2011) 26–35.
[40] Y. Kong, J.N. Hay, Multiple melting behaviour of poly(ethylene terephthalate), Polymers 44 (2002) 623–633.
[41] S.W. Lasoski, W.H. Cobbs, Moisture permeability of polymers. I. Role of crystallinity and orientation, J. Polym. Sci. 36 (1959) 21–33.
[42] D.R. Rueda, A. Varkalis, Water sorption/desorption kinetics in poly(ethylene naphthalene-2,6-dicarboxylate) and poly(ethylene terephthalate), J. Polym. Sci. Part B Polym. Phys. 33 (1995) 2263–2268.
[43] S.A. Jabarin, Crystallization Kinetics of Poly (ethylene Terephthalate). III. Effect of Moisture on the Crystallization Behavior of PET from the Glassy State, J. Appl. Polym. Sci. 34 (1987) 103–108.
[44] T. Negoro, W. Thodsaratpreeyakul, Y. Takada, S. Thumsorn, H. Inoya, H. Hamada, Role of Crystallinity on Moisture Absorption and Mechanical Performance of Role of crystallinity on moisture absorption and mechanical performance of recycled PET compounds, Energy Procedia 89 (2016) 323–327.
[45] J. Wesholowski, A. Berghaus, M. Thommes, Inline determination of residence time distribution in hot-melt-extrusion, Pharmaceutics 10 (2018) 1–10.
[46] E. Reitz, H. Podhaisky, D. Ely, M. Thommes, Residence time modeling of hot melt extrusion processes, Eur. J. Pharm. Biopharm. 85 (2013) 1200–1205.
[47] T. Villmow, B. Kretzschmar, P. Pötschke, Influence of screw configuration, residence time, and specific mechanical energy in twin-screw extrusion of polycaprolactone/multi-walled carbon nanotube composites, Compos. Sci. Technol. 70 (2010) 2045–2055.
[48] L.G. Blok, M.L. Longana, H. Yu, B.K.S. Woods, An investigation into 3D printing of fibre reinforced thermoplastic composites, Addit. Manuf. 22 (2018) 176–186.
[49] S. Wang, L. Daelemans, R. Fiorio, M. Gou, D. D'hooge R., K. De Clerck, L. Cardon, Improving mechanical properties for extrusion-based additive manufacturing of poly(lactic acid) by annealing and blending with poly(3-hydroxybutyrate) 11, Polymers, 2019, pp. 1–13.
[50] Y. Srithep, A. Javadi, S. Pilla, L.-S. Turng, S. Gong, C. Clemons, J. Peng, Processing and characterization of recycled poly(ethylene terephthalate) blends with chain extenders, thermoplastic elastomer, and/or poly(butylene adipate-co-terephthalate), Polym. Eng. Sci. (2011) 1023–1032.
[51] T.A. Osswald, E. Baur, S. Brinkmann, K. Oberbach, E. Schmachtenberg, International plastics handbook, Hanser publishers, 2006. ISBN 9781569903995.
[52] A. Das, A.E.C. Marnot, J.J. Fallon, S.M. Martin, E.G. Joseph, M.J. Bortner, Material extrusion-based additive manufacturing with blends of polypropylene and hydrocarbon resins, ACS Appl. Polym. Mater. 2 (2019) 911–921.
[53] C. Benwood, A. Anstey, J. Andrzejewski, M. Misra, A.K. Mohanty, Improving the impact strength and heat resistance of 3D printed models: structure, property, and processing correlationships during fused deposition modeling (FDM) of poly(lactic acid), ACS Omega 3 (2018) 4400–4411.
[54] X. Gao, D. Zhang, X. Wen, S. Qi, Y. Su, X. Dong, Fused deposition modeling with polyamide 1012, Rapid Prototyp. J. 25 (2019) 1145–1154.
[55] C. Yang, X. Tian, T. Liu, Y. Cao, D. Li, 3D printing for continuous fiber reinforced thermoplastic composites: mechanism and performance, Rapid Prototyp. J. 23 (2017) 209–215.
[56] C. Aumnate, S. Limpanart, N. Soatthiyanon, S. Khunton, PP/organoclay nanocomposites for fused filament fabrication (FFF) 3D printing, Express Polym. Lett. 13 (2019) 898–909.
[57] S.H. Ahn, M. Montero, D. Odell, S. Roundy, P.K. Wright, Anisotropic material properties of fused deposition modeling ABS, Rapid Prototyp. J. 8 (2002) 248–257.
[58] M. Spoerk, J. Gonzalez-Gutierrez, J. Sapkota, S. Schuschnigg, C. Holzer, Effect of the printing bed temperature on the adhesion of parts produced by fused filament fabrication, Plast. Rubber Compos. 47 (2018) 17–24.
[59] J.R.C. Pereira, R.S. Porter, Extrusion drawn amorphous and semi- crystalline poly (ethylene terephthalate): 3. Linear thermal expansion analysis, Polym. (Guildf.) 25 (1984) 869–876.
[60] Spörk, M. Optimisation of the Mechanical Properties and Processing of Polypropylene and Poly(Lactic Acid) Parts Produced by Extrusion-Based Additive Manufacturing, 2018.
[61] J.G. Kovacs, B. Solymossy, Effect of glass bead content and diameter on shrinkage and warpage of injection-molded PA6, Polym. Eng. Sci. (2009) 2218–2224.
[62] Fischer, J.M. Handbook of Molded Part Shrinkage and Warpage; 2003; Vol. 53; ISBN 1–884207-72–3.
[63] M.W. Kim, S.H. Lee, J.R. Youn, Effects of filler size and content on shrinkage and gloss of injection molded PBT/PET/Talc composites, Polym. Compos. (2010) 1020–1027.
[64] G. Wu, J.A. Cuculo, Structure and property studies of poly(ethylene terephthalate)/ poly(ethylene-2,6-naphthalate) melt-blended fibres, Polym. (Guildf.) 40 (1999) 1011–1018.
[65] D. Woods, Effects of crystallization on the glass-rubber transition in polyethylene terephthalate filaments, Nature 174 (1954) 753–754.
[66] I.M. Ward, The mechanical behavior of poly(ethylene terephthalate), J. Macromol. Sci. Part B 1 (1967) 667–694.
[67] N.M.; Alves, J.F.; Mano, E.; Balaguer, J.M.M.; Duen, J.L. Gomez Ribelles, Glass transition and structural relaxation in semi-crystalline poly (ethylene terephthalate): a DSC study, Polym. (Guildf.) 43 (2002) 4111–4122.
[68] C. McIlroy, P.D. Olmsted, Disentanglement effects on welding behaviour of polymer melts during the fused-filament-fabrication method for additive manufacturing, Polym. (Guildf.) 123 (2017) 376–391.
[69] Q. Sun, G.M. Rizvi, C.T. Bellehumeur, P. Gu, Effect of processing conditions on the bonding quality of FDM polymer filaments, Rapid Prototyp. J. 14 (2008) 72–80.
[70] J.E. Seppala, S. Hoon Han, K.E. Hillgartner, C.S. Davis, K.B. Migler, Weld formation during material extrusion additive manufacturing, Soft Matter 13 (2017) 6761–6769.
[71] B.V. Reddy, N.V. Reddy, A. Ghosh, Fused deposition modelling using direct extrusion, Virtual Phys. Prototyp. 2 (2007) 51–60.
[72] M. Spoerk, F. Arbeiter, H. Cajner, J. Sapkota, C. Holzer, Parametric optimization of intra- and inter-layer strengths in parts produced by extrusion-based additive manufacturing of poly(lactic acid), J. Appl. Polym. Sci. 134 (2017) 1–15.
[73] F. Ning, W. Cong, J. Qiu, J. Wei, S. Wang, Additive manufacturing of carbon fiber reinforced thermoplastic composites using fused deposition modeling, Compos. Part B Eng. 80 (2015) 369–378.
[74] E.A. Papon, A. Haque, Tensile properties, void contents, dispersion and fracture behaviour of 3D printed carbon nanofiber reinforced composites, J. Reinf. Plast. Compos. 37 (2018) 381–395.
[75] P. Wolszczak, K. Lygas, M. Paszko, R.A. Wach, Heat distribution in material during fused deposition modelling, Rapid Prototyp. J. 24 (2018) 615–622.
[76] J.F. Rodriguez, J.P. Thomas, J.E. Renaud, Characterization of the mesostructure of fused-deposition acrylonitrile-butadiene-styrene materials, Rapid Prototyp. J. 6 (2000) 175–185.
[77] E.; Polyzos, L.; Pyl, D. Van Hemelrijck, Stochastic modeling of the void shape in 3D-printed thermoplastics, Addit. Manuf. (2021), 102356.
[78] L.A. Northcutt, S.V. Orski, K.B. Migler, A.P. Kotula, Effect of processing conditions on crystallization kinetics during materials extrusion additive manufacturing, Polym. (Guildf.) 154 (2018) 182–187.
[79] J. Gonzalez Ausejo, J. Rydz, M. Musioł, W. Sikorska, M. Sobota, J. Włodarczyk, G. Adamus, H. Janeczek, I. Kwiecień, A. Hercog, et al., A comparative study of three-dimensional printing directions: The degradation and toxicological profile of a PLA/PHA blend, Polym. Degrad. Stab. 152 (2018) 191–207.
[80] B.N. Turner, R. Strong, S.A. Gold, A review of melt extrusion additive manufacturing processes: I. Process design and modeling, Rapid Prototyp. J. 20 (2014) 192–204.
[81] D. Jiang, D.E. Smith, Anisotropic mechanical properties of oriented carbon fiber filled polymer composites produced with fused filament fabrication, Addit. Manuf. 18 (2017) 84–94.
[82] O.S. Carneiro, A.F. Silva, R. Gomes, Fused deposition modeling with polypropylene, Mater. Des. 83 (2015) 768–776.
[83] R.T.L. Ferreira, I. Cardoso, T. Assis, D. Bürger, Experimental characterization and micrography of 3D printed PLA and PLA reinforced with short carbon fibers. *Compos*, Part B 124 (2017) 88–100.
[84] R.A. Wach, P. Wolszczak, A. Adamus-Wlodarczyk, Enhancement of Mechanical Properties of FDM-PLA Parts via Thermal Annealing, Macromol. Mater. Eng. 303 (2018) 1–9.